High Rate Characterization of Three DP980 Steels

Amir Zhumagulov[1], *Armin* Abedini[1], *Taamjeed* Rahmaann[1], *José* Imbert[1 *], *Clifford* Butcher[1], *Michael* Worswick[1], *Skye* Malcolm[2], *Jim* Dykeman[2], *Hesham* Ezzat[3]

[1]Department of Mechanical and Mechatronics Engineering, University of Waterloo, Waterloo, Ontario, Canada
[2]Honda R&D Americas, Raymond, Ohio, USA
[3]Steel Market Development Institute, Auto/Steel Partnership (A/SP), Southfield, Michigan, USA

Abstract. Advanced high strength steels (AHSS) are used extensively in the automotive industry in the ongoing effort to reduce vehicle weight. Their increased strength allows for the reduction of sheet thickness, and thus a reduction in mass, while offering formability and cost advantages when compared to other metal alloys typically considered for lightweight applications. DP980 steels are AHSS being considered for structural energy absorbing components; however, there is a lack of published information on their high rate behaviour. This paper presents the results of an experimental program that characterized three production DP980 steels from three different manufacturers at strain rates of 0.001, 1, 10, 100 and 1,000 s^{-1}. An electro-mechanical frame was used for the quasi-static tests, the 1, 10, and 100 s^{-1} tests were carried out using a fast hydraulic apparatus and the 1,000 s^{-1} experiments were carried out using a tensile split Hopkinson bar. The quasi-static hardening response at strains higher than the uniform elongation of about 7% was obtained by using a shear test, thus avoiding the use of inverse modelling techniques. The results indicate that the DP980 steels are moderately rate sensitive, with one of the materials showing higher sensitivity than the others. One of the materials exhibited a yield point phenomenon that appears to affect the behaviour of the material at 100 and 1,000 s^{-1}, however, the reasons for this behaviour remain an open question. The data was fit to modified Johnson-Cook and Cowper-Symonds model to account for rate sensitivity. The results presented in this paper provide a tool for modelling the dynamic behaviour of DP980 steels.

1 Introduction

Minimizing vehicle weight is a crucial part of modern vehicle design. The reduction of fuel consumption and associated emissions is the primary driver for minimizing vehicle weight. More recently, increased crashworthiness requirements, have increased the drive to reduce the weight of structural components. One way of reducing vehicle weight is by replacing energy absorbing components made from conventional steels with components made from advanced high strength steels (AHSS). Their increased strength allows for the reduction of sheet thickness, and thus a reduction in mass, without compromising safety, while offering formability and cost advantages when compared to other metal alloys typically considered for lightweight applications.

A significant challenge faced by engineers and researchers considering the use of AHSS is the lack of published high rate constitutive data for use in computer aided engineering (CAE). To add to the difficulties, AHSS that are produced by different manufactures can have differences in properties that should be accounted for in CAE predictions. This work aims to provide this data for DP980, a dual phase steel with a nominal ultimate tensile strength (UTS) of 980 MPa. To explore the differences between the products of different manufacturers, a blind testing program of three production DP980 steels from three different manufacturers was performed at rates of 0.001, 1, 10, 100 and 1,000 s^{-1}. This paper presents the experimental procedures and results of these tests, together with the fitting of the data to the Johnson-Cook (JC) [1] and Cowper-Symonds (CS) [2] models. To ensure the constitutive data is suitable for vehicle crash applications, the quasi-static hardening curves are obtained experimentally to strains of 50% using both tensile and shear tests using the methodology recently proposed by Rahmaan *et al.* [3].

2 Experimental Methods and Procedures

The standard JIS specimen geometry shown in Fig, 1-a was used for the 0.001 s^{-1} experiments and the miniature dog-bone (MDB) specimen geometry shown in Fig. 1-b were used for the 1 to 1,000 s^{-1} experiments. The MDB geometry was developed at the University of Waterloo (UW) and has been shown to produce the same results as standard geometries up to UTS [4]. A comparison between the JIS and MDB results obtained in this work

* Corresponding author: jmsimber@uwaterloo.ca

will be shown in the Results and Discussion section. The mini-shear specimen geometry developed by Piers *et al.* [5] (Fig 1-c) was used for the shear experiments. The shear specimens were fabricated at -56° to the TD so that the principal stress direction was aligned with the TD and consistent with the tensile tests.

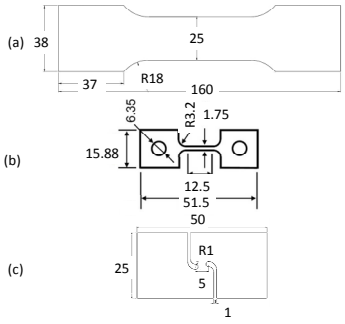

Fig. 1. Specimen geometries used; a) Standard JIS, b) miniature dog-bone and c) mini-shear. All dims in mm.

The shear experiments were performed to obtain tensile constitutive response beyond UTS, following the procedure outlined in [3], the tensile-to-shear stress ratio is computed at the plastic work corresponding to the UTS. Assuming that shear anisotropy does not evolve beyond the UTS work level, this stress ratio is then used to convert the shear stress to an equivalent tensile stress. It is then straightforward to decompose the plastic work into an equivalent strain.

The 0.001 s^{-1} tensile and shear experiments utilized an MTS Criterion 45 electro-mechanical testing machine as shown in Fig. 2. All three specimens were used. The JIS specimens were secured using hydraulic grips. A 100 kN load cell was used to measure the load. The MDB specimens were tested using a 10 kN load cell and specialized grips. The specimens were tested to failure. Specimen strains were measured using *in situ* three dimensional (3D) Digital Image Correlation (DIC), as described below.

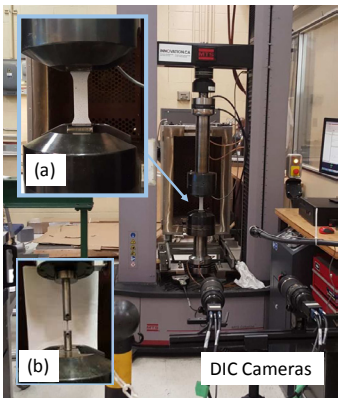

Fig. 2. Quasi-static experimental setup used for the 0.001 s^{-1} tests, shown while testing; (a) JIS and (b) MDB specimens.

The 1, 10 and 100 s^{-1} experiments were conducted using the hydraulic intermediate strain rate (HISR) apparatus, shown in Fig. 3. The apparatus has a 13.3 kN hydraulic actuator with 101.6 mm stroke. The apparatus functions by accelerating the engagement sleeve to a constant velocity which then contacts the engagement piston at the bottom of the stroke as shown in the schematic in Fig. 3. A capacity is used to achieve a maximum stroke rate of 1400 mm/s. A Kistler 9500A4 ±30 kN piezoelectric load cell, which is located directly above the upper grip assembly, measured the load during the test.

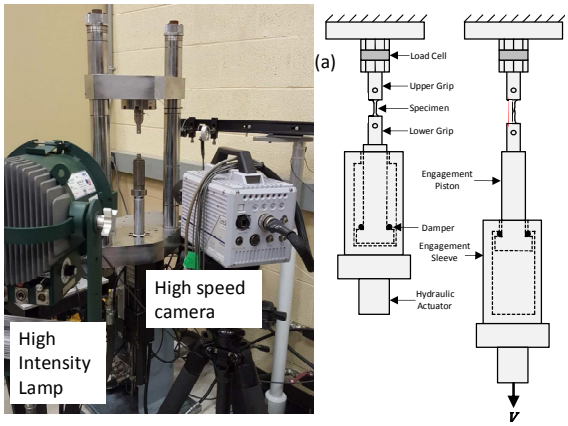

Fig. 3. HISR Apparatus with high speed DIC system.

A tensile split Hopkinson bar (TSHB), shown in Fig. 4, was used for the high rate material testing. Tests were conducted at a nominal strain rate of 1,000 s^{-1}. Samples were mounted on the bar using a high strength adhesive, as shown in Fig 4 (b) and (c). A 455 mm long striker was used. This level of strain did not cause specimen failure on the first loading pulse.

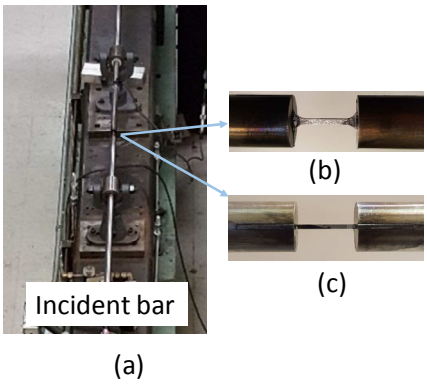

Fig. 4. TSHB apparatus used for this work. Insets b) and c) show side and top views of the sample bonded in position.

Specimen deformation was directly measured using stereoscopic DIC in the MTS and 2D DIC in the HISR. Each specimen was first painted white and then painted with a randomized black speckle pattern. The tests were recorded and then the images were analysed using DIC software by Correlated Solutions. For the MTS tests, two Point Grey Gazelle cameras were used, recording at a frame rate of 1 frame per second (fps). For the HISR tests, a Photron SA5 high speed camera was used to capture the images at a rate of 2,000, 15,000 and 70,000 fps for the 1, 10 and 100 s^{-1} tests, respectively. A virtual strain gauge length of 0.3 mm was used throughout. During the tests, the Correlated Solutions DIC data acquisition system was used to capture the force data

from the load cell for each recorded image. After post-processing was completed, a user defined virtual extensometer was used to determine the engineering strain. The strain fields in the mini-shear specimens were analysed using the detailed procedures described in [3].

The stress-strain response of the Hopkinson bar specimens was determined using the standard analysis following [6].

3 Results and Discussion

3.1 Experimental Results

The materials were first tested at 0.001 s^{-1} using the JIS samples to determine the baseline low-rate properties. The results are presented in Fig. 5, where it can be seen that the materials exhibited similar, yet distinct behaviours. Material 1 had the highest UTS, Material 2 had the most distinct behaviour due to the presence of yield point phenomenon, and Material 3 had a UTS similar to Material 2, but with the yield behaviour of Material 1.

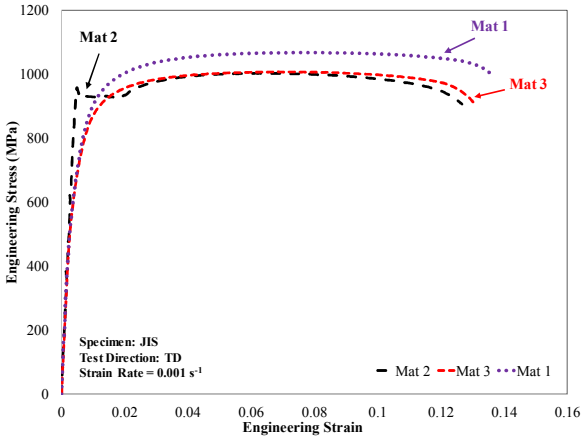

Fig. 5. Average curves for the 0.001 s^{-1} results of each material.

Given that the intermediate and high rate tests were performed with the MDB specimen, a comparison was made between data obtained from the JIS samples and data obtained with MDB specimens tested at 0.001 s^{-1}. Fig. 6 shows this comparison for Material 2 and it can be seen that the MDB results are essentially equal to the JIS results, at least up to the onset of necking. The comparisons for the other two materials were similar, but are not shown for brevity. Material 2 was chosen for presentation because it had the most complex behaviour.

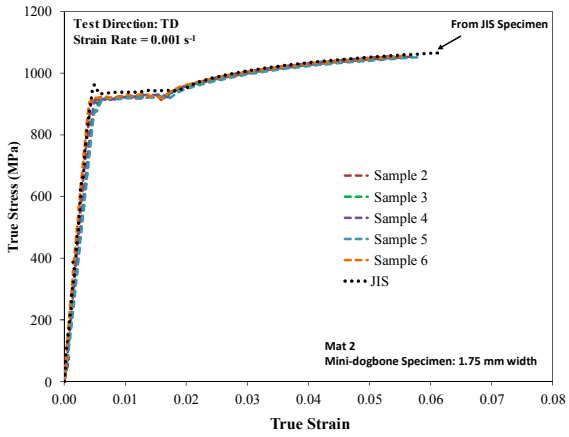

Fig. 6. Comparison of the average 0.001 s^{-1} results obtained with the JIS specimens with six tests performed with the MDB sample.

The engineering stress-strain data for Material 2 at 1, 10, 100 and 1,000 s^{-1} are shown in Figs. 7 to 10, together with an average curve, to show the data and the repeatability of the tests. The data for Materials 1 and 3 is of similar repeatability; however, the 100 and 1,000 s^{-1} data for Material 2 showed some oscillations that were not present in Materials 1 and 3. The oscillations observed in the Material 2 results are attributed to the yield point phenomenon observed, but a complete investigation of their cause was beyond the scope of this work. The full data set for Materials 1 and 3 is not shown for brevity.

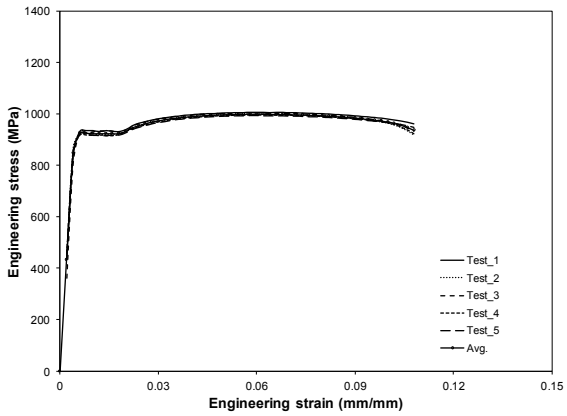

Fig. 7. Experimental engineering stress strain for Material 2 at 1 s^{-1}.

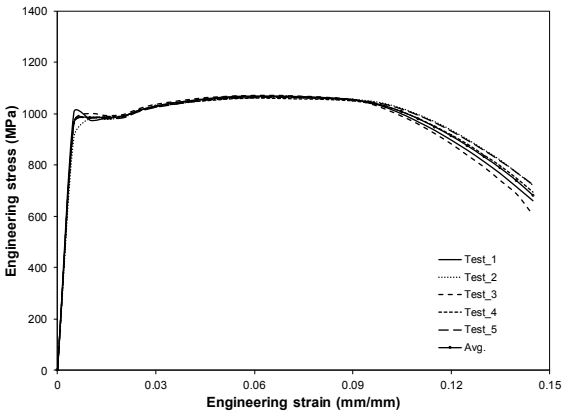

Fig. 8. Experimental engineering stress strain for Material 2 at 10 s^{-1}.

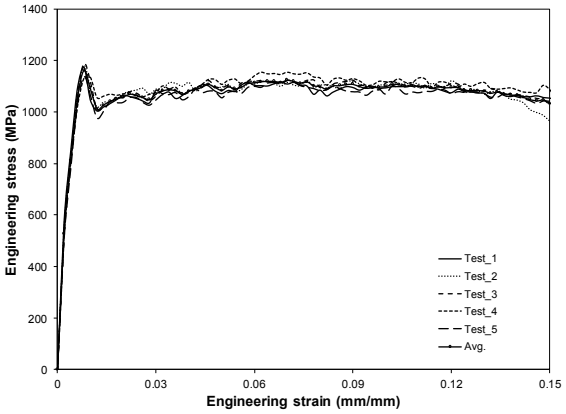

Fig. 9. Experimental engineering stress strain for Material 2 at 100 s^{-1}.

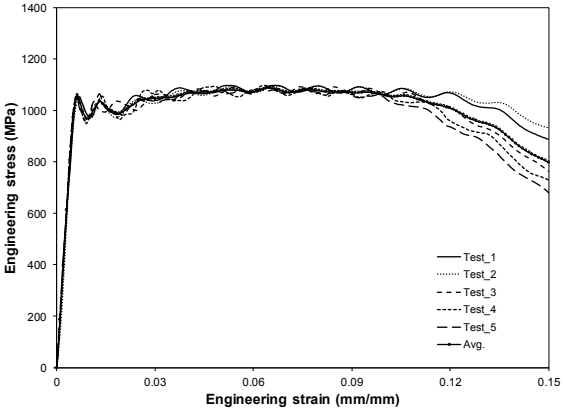

Fig. 10. Experimental engineering stress strain for Material 2 at 1,000 s^{-1}.

The shear and true tensile stress as a function of plastic work is shown for a nominal von Mises equivalent strain rate of 0.001 s^{-1} is presented in Fig. 11 for Material 1. The tensile work is computed until the UTS whereas the work in shear is computed until the peak load is reached. The clear advantage of the shear test is that it does not experience localization and is valid to large strain levels. The shear-extrapolated data is show below.

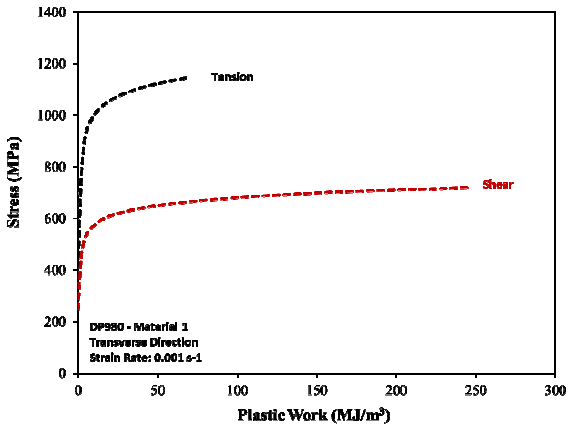

Fig. 11. Comparison of true tensile and shear stress versus plastic work for Material 1.

A plot showing the strain rate sensitivity of all three materials is shown in Fig. 12, which shows the true stress at 6% true strain for each strain rate tested. Each data point is the average of five repeat tests. All three materials showed moderate strain rate sensitivity, with Material 3 showing a slightly higher sensitivity.

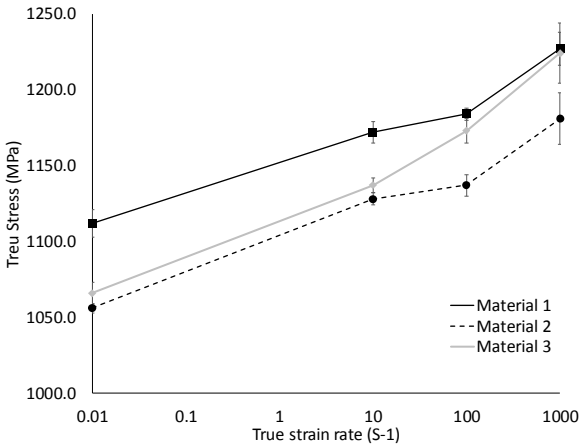

Fig. 12. Experimental strain sensitivity of each material studied. The average true stress at 6% true strain is presented. The length of the error bar is equal to the standard deviation from the mean.

3.2 Constitutive Fits

The experimental data was fit to the following constitutive equation,

$$\bar{\sigma}\left(\varepsilon^p, \dot{\varepsilon}^p\right) = \bar{\sigma}_{qs}\left(\varepsilon^p\right) \cdot f\left(\dot{\varepsilon}^p\right) \quad (1)$$

where $\bar{\sigma}_{qs}\left(\varepsilon^p\right)$ is the quasi-static flow stress response given by a Holloman equation,

$$\bar{\sigma}_{qs} = K(\varepsilon^p)^n \quad (2)$$

and $f(\dot{\varepsilon}^p)$ is a scaling function for strain rate dependence that was used to examine the rate sensitivity in the constitutive response by fitting the single parameter form Johnson-Cook (JC) rate sensitivity [1] given by,

$$f_{JC}(\dot{\varepsilon}^p) = 1 + C\ln\left(\frac{\dot{\varepsilon}^p}{\dot{\varepsilon}_0}\right) \tag{3}$$

and to the Cowper-Symonds (CS) model [2] given by;

$$f_{CS}(\dot{\varepsilon}^p) = 1 + \left[\frac{1}{D}\ln\left(\frac{\dot{\varepsilon}^p}{\dot{\varepsilon}_0}\right)\right]^{\frac{1}{P}} \tag{4}$$

where $\dot{\varepsilon}^p$ = effective plastic strain and $\dot{\varepsilon}_0 = 0.001\ \text{s}^{-1}$.

The model constants fit to the data are shown in Table 1.

Table 1. Model constants for the Holloman equation, JC and CS models.

Material			Johnson-Cook	Cowper-Symonds	
	K (MPa)	n	*C*	*D*	*P*
DP980 - 1	1392	0.074	0.00558	49.310	0.52125
DP980 - 2	1233	0.053	0.00643	47.362	0.53445
DP980 - 3	1318	0.073	0.01005	31.884	0.45893

The resulting constitutive fits for each DP980 material at 0.001 s^{-1} are shown in Fig. 13 along with the simple Holloman law (Eq. 2) calibrated to 50% strain. This data includes both the tensile and shear data at this rate, showing the extrapolation to large strains enabled by the shear specimen. This calibration was then combined with either the JC (Eq. 3) and CS (Eq. 4) scaling factors to account for rate sensitivity.

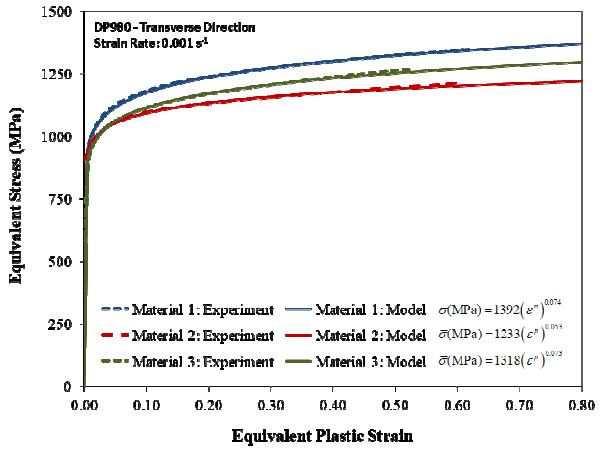

Fig. 13. Experimental strain sensitivity of each material studied.

Fig. 14 serves to compare the measured strain rate sensitivity of Material 2 with the predictions from the JC model. The predictions for the other materials were of similar quality.

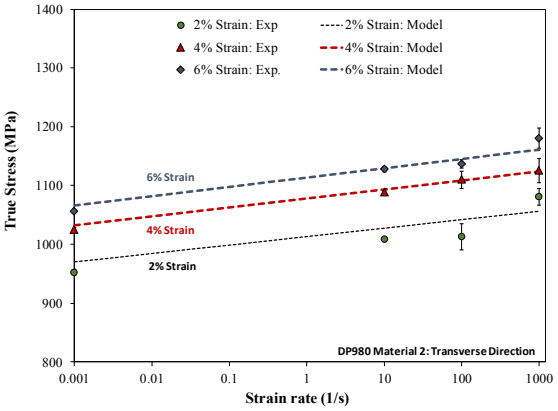

Fig. 14. Experimental rate sensitivity of Material 2 compared to the J-C model predictions.

The CS predictions are compared to the measured data for Materials 1-3 in Figs. 15-20. In general, the fit quality was deemed superior using the CS rate sensitivity term. The greatest discrepancy between the model and the experiments occurred for Material 2 due to the presence of the yield point phenomenon, as can be seen in Fig. 17.

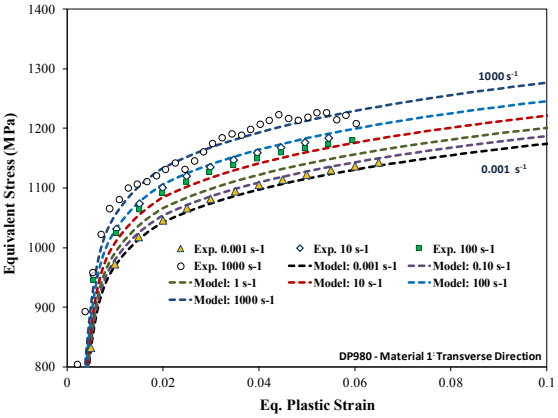

Fig. 15. Comparison of experimental and CS predicted equivalent stress and equivalent plastic strain for Material 1.

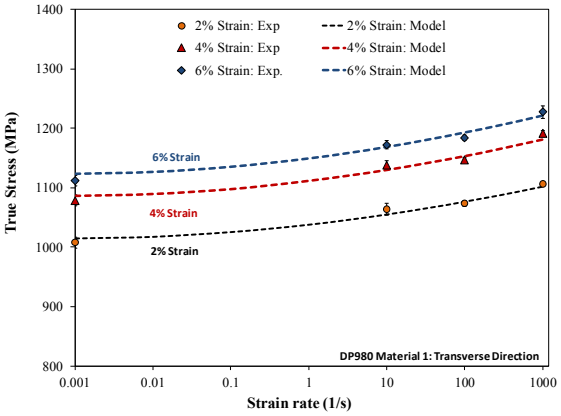

Fig. 16. Experimental rate sensitivity of Material 1 compared to the CS model predictions.

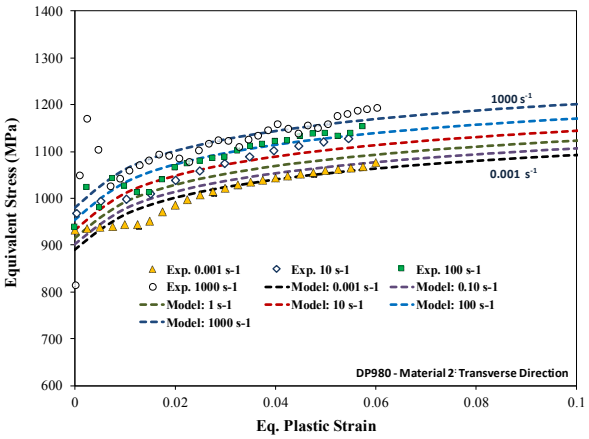

Fig. 17. Comparison of experimental and CS predicted equivalent stress and equivalent plastic strain for Material 2.

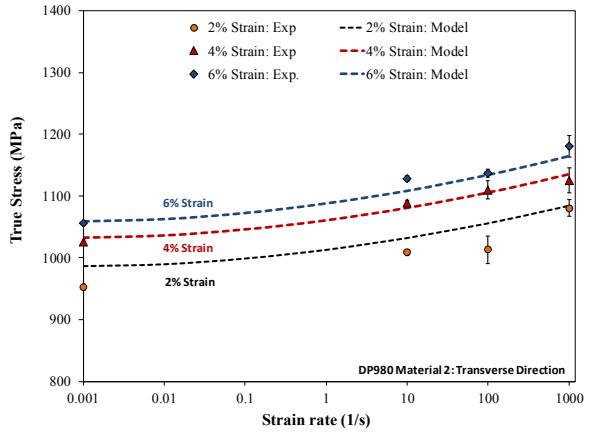

Fig. 18. Experimental rate sensitivity of Material 2 compared to the CS model predictions.

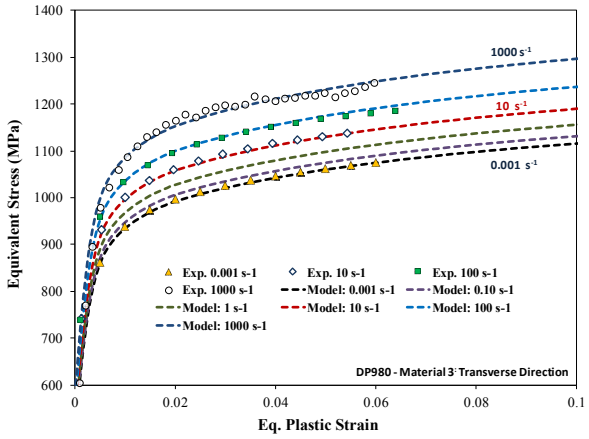

Fig. 19. Comparison of experimental and CS predicted equivalent stress and equivalent plastic strain for Material 3.

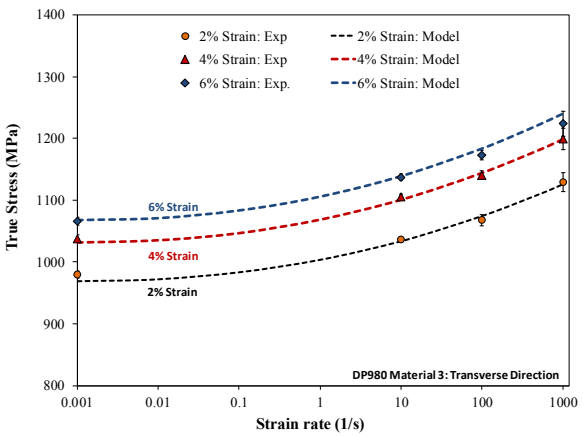

Fig. 20. Experimental rate sensitivity of Material 3 compared to the CS model predictions.

4 Conclusions

The high rate constitutive behaviour of three commercial DP980 steels was determined by testing the materials at 0.001, 1, 10, 100 and 1,000 s^{-1}. All materials showed moderate strain rate sensitivity. Although generally similar, noticeable differences were observed, namely the presence of yield point phenomena in Material 2. Material 3 seem to have a slightly higher strain rate sensitivity. The data was fit to the JC and CS rate sensitivity terms, with the latter being able to reproduce the experimental data somewhat more accurately. The data and models presented in this paper provide a useful tool for modelling the dynamic behaviour of DP980 steels.

The authors greatly appreciate the financial support SMDI for this work.

References

1. J. Cook and W. Cook, Eng. Frac. Mech., **21-1** (1985)
2. G. Cowper, P. Symonds, App. Math. Rep., **28** (1957)
3. T. Rahmaan, A. Abedini, C. Butcher, N. Pathak, M.J. Worswick, Int. J. Imp.Eng. **108** (2017)
4. R. Smerd, S. Winkler, C. Salisbury, M. Worswick, D. Lloyd, M. Finn, Int. J. Impact. Eng., **32** (2005)
5. J. Peris, P., Verleysen, J. Degrieck, Exp. Mech. **52**
6. R. Grey III, ASM, v8, Mech. Testing and Eval. (2000)